# TRACKING LOW-LEVEL CLOUDS OVER LAND ON METEOSAT IMAGES

André Szantai, Françoise Désalmand, Michel Desbois, Pascal Lecomte

Laboratoire de Météorologie Dynamique, Ecole Polytechnique, 91128 Palaiseau, France

Patrick Perez, Stelios Zimeras, Patrick Bouthemy

IRISA, Campus de Beaulieu, 35042 RENNES, France

ABSTRACT

The tracking of reliable low-level cloud motion winds over land remains a difficult task. For this purpose, conventional computation techniques can be used and be associated to selection tests on vectors based on climatological characteristics of the expected winds. Such tests have been successfully used to extract monsoon winds over West-Africa during the rainy season from Meteosat VISible images. The number of vectors is increased by using rapid scan images. Other improvements include the use of the information from other channels (in particular the Water Vapour) to reject non low-level winds.

Methods based on the estimation of quasi-dense motion fields using optical flow techniques are introduced. Generic methods have been adapted to the highly deformable nature of cloud motion and to the photometric specificities of images at hand (low contrast and global variations of illuminations). Results of both types of methods are presented and compared.

## 1. Introduction

The tracking of low-level clouds over land has been considered as an almost impossible task at the nominal resolution of current Meteosat satellites (30 min between images), due to the short lifetime of these clouds and often to their small size (generally less than the size of a VISible pixel). Therefore low-level cloud motion winds (CMWs hereafter), when they are produced, are not used for assimilation or forecast in models over land (Ottenbacher et al., 1997). This study shows in section 2 that a limited number of CMWs associated to the monsoon flow over West-Africa can nevertheless be computed during the rainy season with images of Meteosat 7. In section 3, a test based on the correlation between the content of infrared (IR) and the water vapour (WV) channels is presented. This test can be used to eliminate vectors associated to high-level clouds. Section 4 shows the effect of using a reduced time interval between images on the number of low-level CMWs. In section 5, new techniques based on the computation of the optical flow enable the construction of dense cloud motion vector fields. Preliminary results obtained with these techniques are compared qualitatively with those obtained by the "classical" CMW computation method.

## 2. Statistics of cloud motion winds obtained with current Meteosat data

In this first step, we have tried to extract low-level CMWs associated to the monsoon flow over West-Africa during the summer months (rainy season) of 1998, with the standard temporal resolution of 30 min between images. A preliminary study (Désalmand et al., 1999) has shown that the visible (VIS) channel of Meteosat (with a solar angle correction) enabled a better tracking of low-level clouds than the IR channel. For this purpose, CMWs are computed on a regular grid with a standard method from a triplet of images:

- 2 raw wind fields are computed from image pairs (1, 2) and (2, 3). Displacements are obtained by minimising the Euclidean distance.
- Quality tests remove too small and too large vectors and collocated vectors in both fields with a large difference in direction and / or speed (temporal symmetry check).

Specific tests are then applied to extract low-level winds:

- Low level winds are selected with the help of the IR brightness temperature of the 10 % coldest pixels located inside the target window (BTIR). CMWs associated to a BTIR below a threshold value of 0°C are considered as medium- or high-level winds and therefore are excluded.
- Low level CMWs with a direction between 150 and 270° are then selected. These values correspond approximately to the climatological limits of the direction of the monsoon flow, which is observed over West Africa.

Each CMW which has successfully passed the previous tests is compared to its neighbour(s), if available (spatial symmetry check). If at least one neighbour vector with close characteristics is present, the tested CMW is considered eventually as a monsoon wind.

These quality tests do not take into account WV located above the clouds (which can reduce the observed $BT_{IR}$ by a few degrees K), nor effects related to the partial coverage of a pixel by small clouds or to the semi-transparency of high-level clouds. A visual observation of IR images with the selected VIS CMWs shows that a minority of these winds are related to cirrus clouds associated to the outflow at the top of convective clusters. Such inconsistent vectors are tolerated at this stage because the main goal of this study is to show that the extraction of low-level winds over land is feasible.

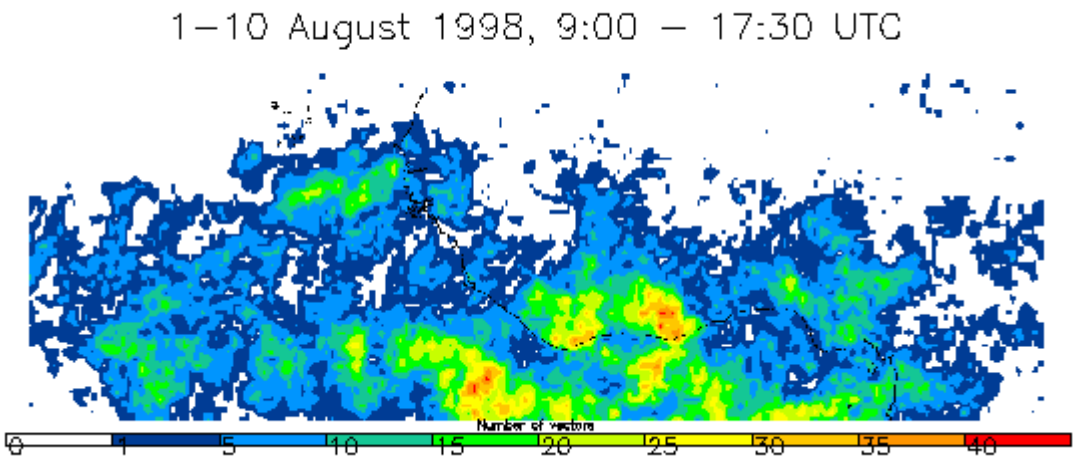


Figure 1. Isolines of the number of monsoon CMWs for the first ten-day period of August 1998.

Figure 1 represents the number of monsoon CMWs over West-Africa between 1 and 10 August 1998. Although the monsoon flow is a quasi-permanent feature of the atmospheric circulation in this area at this time of the year, it appears that the proportion of monsoon CMWs is small, compared to the number of theoretically possible observations (less than 26 %, for a possible maximum of 170 vectors at each grid point). This confirms the difficulty of tracking low-level clouds over land (furthermore high-level clouds which are part of mesoscale convective clusters mask the motion located at lower levels in some areas). Monsoon CMWs are frequently measured in specific, mainly lowland areas: over Ghana, the Ivory Coast and at a lesser extent over Nigeria. The same preferential locations have been observed during another ten-day period (1-10 July 1998), with fewer vectors.

## 3. Selection of low level CMWs with the IR/WV correlation

The correlation between the IR and WV pixel values over a limited area can be used to indicate the presence of high-level clouds (Xu et al., 1998). Therefore, we have computed the IR/WV correlation over the area covered by the target window used for the calculation of each (VIS) CMW. For the studied case (2 Aug. 1998, 12:00-12:30 UTC), the same methodology as in section 2 has been applied, but without any selection on the direction of the CMWs. It appears that a vast majority of low-level CMWs correspond to a low IR/WV correlation values (below 0.5). A few vectors with a high correlation value are associated to the motion of cirrus clouds. On the other hand, some vectors have a high correlation but have neighbours with low correlation values: in these cases, the motion of low-level clouds is measured below cirrus clouds. These cirrus are thin enough in the VIS channel to enable the calculation of a CMW but thick enough to be detected in the IR and WV channels (thus the high IR/WV correlation values).

The use of the IR/WV correlation as a selection criterion of low-level CMWs has been investigated on another case (5 July 1998, 12:00-12:30 UTC). The set of 1293 low-level CMWs selected with the test on the brightness temperature ($BT_{IR}$ ³ 0°C) is compared to the 1377 CMWs selected with their low IR/WV correlation value (² 0.4) only (without applying the brightness temperature test, all other quality tests being the same). It appears that a vast majority of vectors is common to both sets (Figure 2). The vectors selected only by the correlation generally have a large speed and are related to high-level clouds.

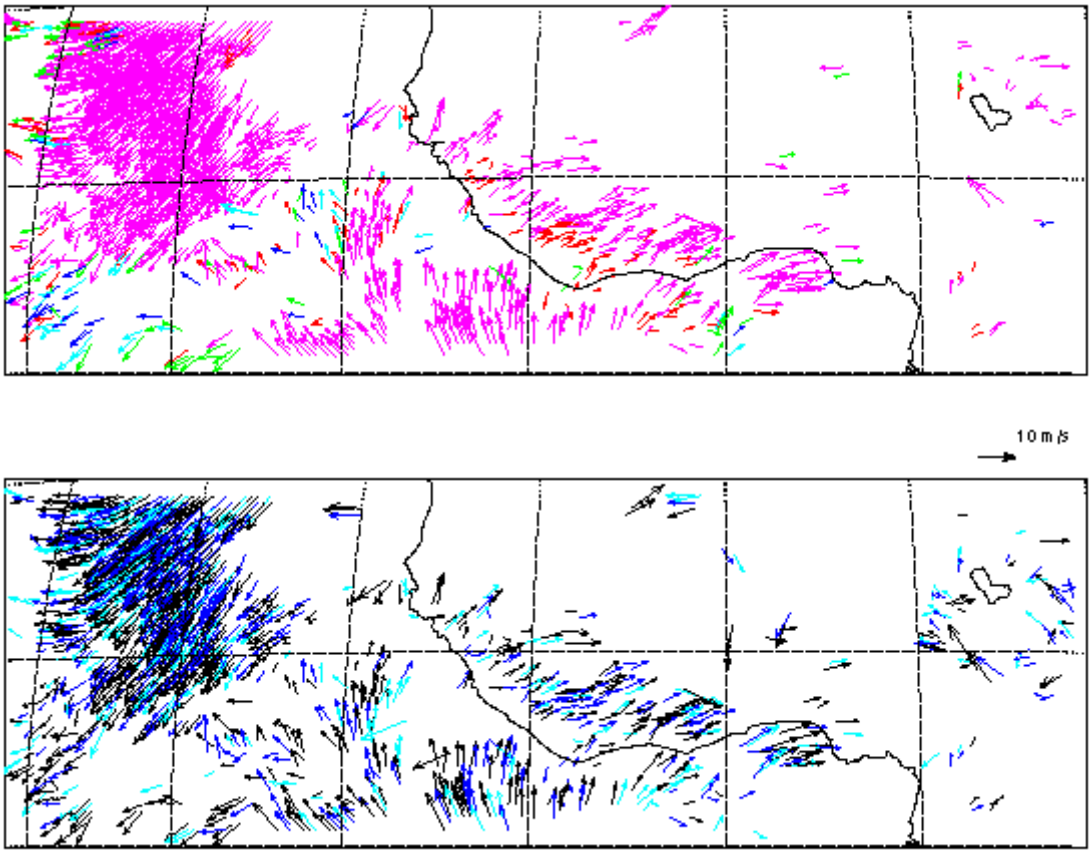


Figure 2. Top: vectors with high $BT_{IR}$ (1293 vectors. Colour scale: blue - green - red - pink, with increasing brightness temperature above 0°C). Bottom: vectors with low IR/WV correlation (1377 vectors. Colour scale: black - dark blue - light blue, with increasing correlation, below 0.4).

From these two examples, we conclude that both tests extract almost similar sets of low-level CMWs.

But the $BT_{IR}$ test is more efficient to remove high-level winds, and is also able to retain low-level winds measured under high-level (thin) cirrus clouds.

## 4. Cloud motion winds from rapid scan images

The effect of a reduced time interval between images on the number of low-level CMWs has been investigated with a series of Meteosat 6 images covering one day (28 July 1999) during daytime, with a 7.5 min time interval (rapid scan). These images centred on the equator cover the central Atlantic Ocean and West/Central-Africa. Three series of low-level CMWs have been computed with time intervals of 7.5, 15 and 30 minutes between images, with the same quality tests as in section 2 (with thresholds adapted to the reduced time interval and without selection on the wind direction).

Figure 3 shows the huge increase in the number of vectors when the time interval is reduced from 30 to 15 minutes (724 vs. 2592 vectors over land and over ocean). This number is further increased when a 7.5 min interval is used (3323 vectors). This increase in the vector number with the reduction of the time interval can be observed over land during the whole period of the study (figure 4). The fact that the lifetime of small low-level clouds, especially cumulus, is around 10-15 min and is closer to the reduced time intervals than the nominal 30 min between current Meteosat images can explain this increase in the number of vectors. The decrease observed after 11:00 UTC with 7.5 and 15 min time intervals can be explained by increased convection producing more convective cloud systems reaching high altitudes, and by the onset of dusk, which moves from east to west with time.

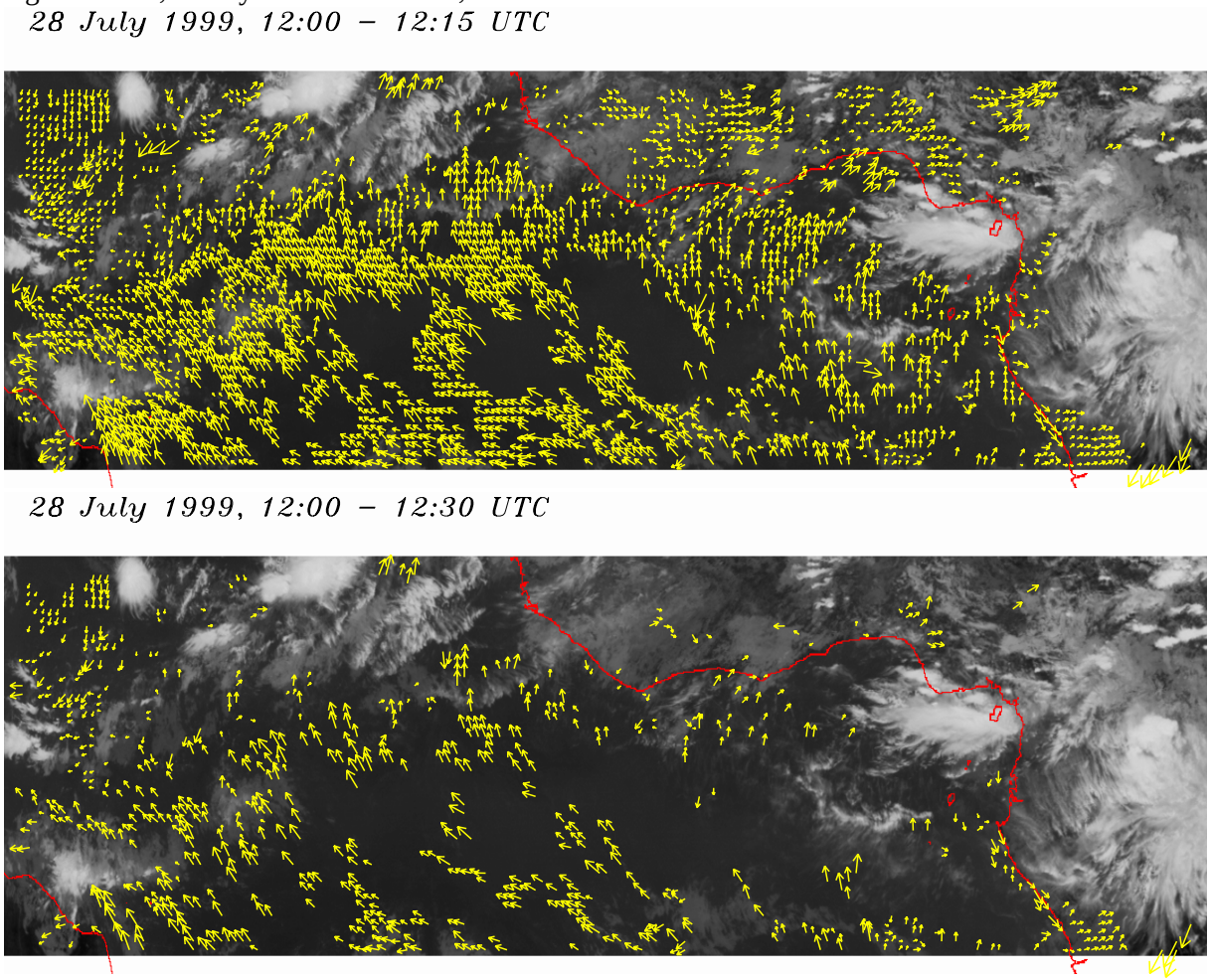


Figure 3. Low-level CMW fields with 30 min (bottom) and 15 min (top) time intervals, with the 12:00 UTC IR image.

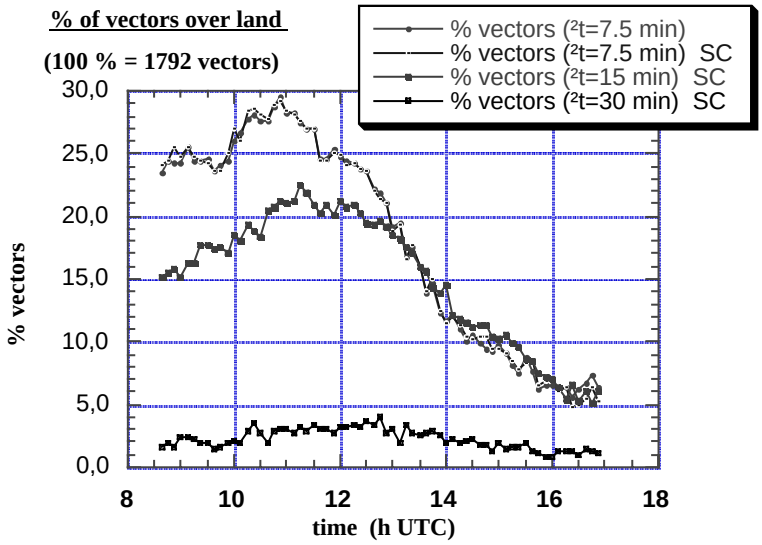


Figure 4. Percentage of vectors over land with different time resolutions (7.5 min : with (SC) and without correction of the solar angle, 15 and 30 min : with correction only (SC).

The effect of a solar correction of images (correction of the solar zenith angle) with a 7.5 min time interval has also been investigated. For such short time intervals, it appears that the number of selected CMWs is almost identical with and without a solar correction (top curves of figure 4). Very close solar illumination on a pair of images at any location explains that reliable CMWs can be computed with uncorrected images. (With a solar correction, CMWs cannot be computed reliably in the areas where the solar zenith angle reaches its maximal value, set to 75°. CMWs with higher values have nevertheless been computed, but without image correction.)

## 5. Dense vector fields

From an image processing point of view, the movement of the clouds leads to a spatial variation of the image or a sequence of images. The variation of the image introduces a motion at different instants. An effective way to extract information or to identify the shape of an object is to use the *optical flow*. An optical flow can be defined as *the transformation of the 3D motion of objects and cameras to a 2D motion on the image plane via a suitable projection system*. The presentation of the optical flow as a vector-values functions of continuous spatial co-ordinates can be defined as a motion field.

The main steps of the motion field modelling are introduced by:

1. Modelling the motion as a cost energy function including observation constraints and smoothness terms (Horn and Schunck, 1981),
2. Expressing the optical flow as a model, constant or affine (Stiller and Konrad, 1999),
3. Introducing robustness to reduce the differences between the data and the optic flow model,
4. Minimise the energy function using a general hierarchical optimisation framework, which is both multiresolution and multigrid with an adaptive way (Memin and Perez, 1998).

### 5.1 Modelling of the motion field

Let us define the unknown 2D motion field as ={s, s∈S} over a rectangular pixel lattice S and the intensity function at two consecutive instants t and t+1 as f(t)={f(s,t), s∈S}. Assuming a temporal constancy of the brightness, the optical flow constrained equation (OFCE) is given by:

$$\nabla \boldsymbol{f}(\boldsymbol{s},\boldsymbol{t})\omega_s + \boldsymbol{f}_t(\boldsymbol{s},\boldsymbol{t}) = \boldsymbol{0}$$

where, $\nabla f$ represents the spatial gradient of f with $\nabla \boldsymbol{f} = \left(\boldsymbol{f}_x, \boldsymbol{f}_y\right)^T$ and $f_t(s,t)$ is the temporal partial derivative of luminance f. The model assumes small displacements. The global estimation of the motion field can be achieved by optimising the following cost function (from Horn and Schunck (1981)):

$$\boldsymbol{U}(\omega, \boldsymbol{f}) = \sum_{s \in S} \left[\nabla \boldsymbol{f}(\boldsymbol{s},\boldsymbol{t})\omega_s + \boldsymbol{f}(\boldsymbol{s},\boldsymbol{t})\right]^2 + \boldsymbol{a} \sum_{<s,r> \in C} \left\|\omega_s - \omega_r\right\|^2$$

where, S is the set of pixel grid, C are the possible cliques for the neighbouring sites <s,r> (the 4-neighbourhood system in this case), and a>0 is the smoothing parameter controlling the balance between the two terms. The first term represents the interaction between the field (unknown variables) and the data (given variables), where the second term expresses the smoothness constraint. The disadvantages of this formulation are:

- The OFCE is not valid in case of large displacements, because of the linearisation,
- The real field is not globally smooth, containing probably discontinuities that might not be presented because of the quadratic cost function.

### 5.2 Robust estimators

To efficiently cope with the large deviations from the data model and the prior model, robust functions (Black and Anandan, 1996) are introduced and more precisely robust M-estimators. After this modification, the cost function takes the form:

$$\boldsymbol{U}(\boldsymbol{d}\omega, \boldsymbol{f}) = \sum_{s \in S} \rho_1\left[\nabla \boldsymbol{f}(\boldsymbol{s},\boldsymbol{t})\omega_s + \boldsymbol{f}(\boldsymbol{s},\boldsymbol{t})\right]^2 + \boldsymbol{a} \sum_{<s,r> \in C} \rho_2\left\|\boldsymbol{d}\omega_s - \boldsymbol{d}\omega_r\right\|^2$$

where, $\rho_1$ and $\rho_2$ are the two robust estimators (in this case the Leclerc estimator was used) and $d_\omega$ is the incremental displacement field. According to minimisation aspects, for the estimators (Black and Anandan, 1996; Geman and Reynolds, 1992), the cost function takes the form:

$$\boldsymbol{U}(\boldsymbol{d}\omega, \boldsymbol{f}) = \sum_{s \in S} \delta_s\left[\nabla \boldsymbol{f}(\boldsymbol{s},\boldsymbol{t})\boldsymbol{d}\omega_s + \boldsymbol{f}(\boldsymbol{s},\boldsymbol{t})\right]^2 + \phi_1(\delta_s) + \boldsymbol{a} \sum_{<s,r> \in C} \beta_{sr}\left|\boldsymbol{d}\omega_s - \boldsymbol{d}\omega_r\right|^2 + \phi_2(\beta_{sr})$$

where, $\delta_S$ are the weights of the data that controls the optical flow constrained equation and $\rho_{Sr}$ are the weights that controls the velocity discontinuities.

### 5.3 Multiresolution-Multigrid approaches

For each instant t of the sequence, a pyramid of images $\{f^{(k)}\}$ is derived by successive Gaussian smoothing and regular resampling by a factor of 2. At coarsest level, displacements are reduced and cost function can be used. For the next resolution levels, only one incremental $d\omega^{(k)}$ is estimated to refine estimate $\hat{\omega}^{(k)}$, obtained from the previous level. The cost function depends on from three parameters: $r_1$, $r_2$ and $r_3$ that are approximately defined by the variances of the three robust models (interaction between the field and the data and smoothness constraints between different neighbouring structures).

For a faster convergence of the minimisation process, a multigrid approach is applied. The process partitions the image into lattice of size $2^{(k)}$ at the grid level k. The cost function can then be expressed according to the partition and a parametric model is estimated as an increment on each pixel. The displacement increment estimated on a pixel depends on the total displacement on the neighbourhood of this pixel; that implies the field could be continuous between the pixels and in this case no block effects are appeared.

When the grid level is changed, the partition of the grid is also changed (in an adaptive way). The number of blocks could be the criterion to measure the way the model fits the data or could be used as a prior knowledge for the structure of the particular application. Using this adaptive way of splitting the blocks, eventually there is a distinction between the regions of interests, where the estimation must be accurate, and the regions where information is useless.

### 5.4 Extension of the standard method

When the luminance is constant along its trajectories, the standard methods (see above) can be applied to estimate the optical flow field. This assumption is not valid in cases of spatial and temporal distortions as in fluid image sequences. As an extension, a new model is applied based on the continuity equation of fluid mechanics and a smoothness function considering the divergence and vorticity (curl) of the motion field. The basic idea is to have different penalisation for div(ω) and curl(ω) in the smoothness terms, to encourage one or the other quantity.
In this case the cost energy function takes the form:

$$U(d\omega, f) = \sum_{s \in S} \rho_1 \left[ \nabla f(s,t) d\omega_s \exp\left[ div(\omega_s) \right] + f(s,t) \right]^2 + \alpha \sum_{<s,r> \in C} \rho_2 \left\| d\omega_s - d\omega_r \right\|^2 +$$
$$\lambda \sum_{s \in S} \rho_2 \left[ \left\{ div(\omega_s) - L_{div_s} \zeta_{div_s} \right\}^2 + \left\{ curl(\omega_s) - L_{curl_s} \zeta_{curl_s} \right\}^2 \right]$$

where $div(\omega_S)$ can be expressed as a product of two factors: $L_{div}$ and $\xi_{div}$, $\lambda>0$ is a control parameter between the two factors of smoothness term.

### 5.5 Results

A dense vector field, which represents the motion of clouds at all levels, has been calculated with the improved method described above (28 July 1999, 12:00 - 12:07 UTC). On figure 5, the corresponding chart can be compared with the low-level CMW field obtained with the same images and the method described in sections 2 and 4. On both charts, the vectors show the same direction of motion. But more complete (quantitative) comparisons must be undertaken, especially in the areas where low- and high-level clouds are in contact.

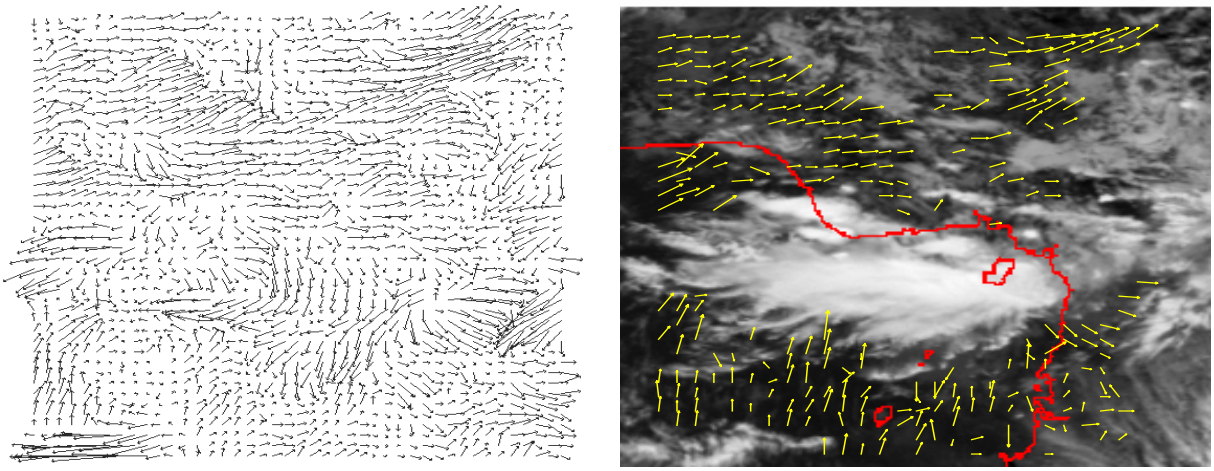

Figure 5: dense vector field calculated with the optical flow method (left) and low level CMWs obtained with the classical method (right, with IR image of 28 July 1999, 12:00 UTC)

## 6. Conclusion and prospects

This study confirms that a limited number of low-level CMWs can be computed over land in the tropics from VIS images with the time interval of 30 minutes between images, available on current Meteosat satellites. An important increase in the number of CMWs is observed when the time interval is reduced to 15 minutes and can be expected from future Meteosat Second Generation satellites which will have that time interval in operational mode. A further but smaller increase is observed during a part of daytime when the time interval is reduced to 7.5 minutes. In the latter situation, CMW fields are

almost identical whether a solar correction is applied or not; therefore we suggest suppressing this preliminary image processing.

The IR/WV correlation has been tested as an alternate parameter for the selection of low-level CMWs. It appears that the use of the IR brightness temperature (high values) enables a slightly better selection than the correlation (low values), but that a large majority of vectors are retained by both selection tests. Future improvements of the selection method are planned, they include a better height assignment and a semi-transparency correction.

A new method based on optical flow determination has been developed for the construction of dense cloud motion fields. A qualitative comparison shows that vectors in areas where low-level clouds are present have directions similar to the (limited number of) vectors available with conventional techniques. Quantitative comparisons in a near future will evaluate the quality of this method.

## ACKNOWLEDGEMENT

This study was realised partly under EUMETSAT contract no. EUM/CO/99/699/KTH. The authors would also like to thank EUMETSAT for the financial help that enabled one of them to attend to this Winds Workshop.

## REFERENCES

Black, M. and P. Anandan (1996). The robust estimation of multiple motions: parametric and piecewise smooth flow fields. *Computer Vision and Image Understanding*, **63**, 1, pp 75-104.

Désalmand, F., A. Szantai and M. Desbois (1999). An attempt to retrieve low cloud motion winds over land in the African monsoon flow on Meteosat pictures. *Geophys. Res. Lett*., **26**, pp 319-323.

Horn, B. K. P. and B. G. Schunck (1981). Determining optical flow. *Artificial Intelligence*, **17**, pp 185-203.

Memin, E. and P. Perez (1998). Optical flow estimation and object-based segmentation with robust techniques. *IEEE Trans. Pattern Anal. Machine Intell.*, **7, 5,** pp 703-719.

Ottenbacher, A., M. Tomassini, K. Holmlund, and J. Schmetz (1997). Low-level cloud motion winds from Meteosat high resolution visible imagery. *Wea. Forecasting* , **12**, pp 175-184.

Stiller, C. and J. Konrad (1999). Estimating motion in image sequences. *IEEE Signal Processing Magazine*, **16, 4**, pp 70-91.

Xu, J., Z. Qisong, F. Xiang and L. Jian (1998). Cloud motion winds from FY-2 and GMS-5 meteorological satellites. *Proc. Fourth International Winds Workshop*, Saanenmőser, Switzerland (20-23 Oct. 1998). Eds. JMA, EUMETSAT, WMO and NOAA. EUMETSAT : pp 41-48.